Introduction to sparse-data X-ray tomography: Part C

Samuli Siltanen

Department of Mathematics and Statistics
University of Helsinki, Finland
samuli.siltanen@helsinki.fi
www.siltanen-research.net

IMPA, Rio de Janeiro, Brazil
Symposium on Inverse Problems in Science and Engineering
October 24–27, 2017

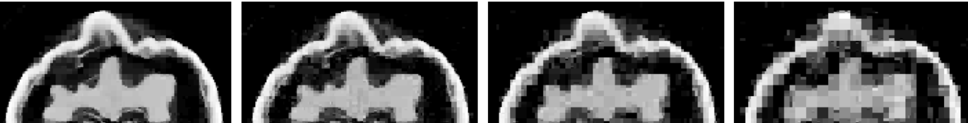

Outline

This part of the talk is a joint work with

Kati Niinimäki, University Paris-Sud, France

Matti Lassas, University of Helsinki, Finland

Keijo Hämäläinen, University of Helsinki, Finland

Aki Kallonen, University of Helsinki, Finland

Ville Kolehmainen, University of Eastern Finland

Esa Niemi, University of Helsinki, Finland

How to choose the regularization parameter in the total variation (TV) functional?

Heuristics: Rullgård **2008**

Balancing ℓ^1 and TV: Clason, Jin & Kunisch **2010**

Local variance: Dong, Hintermüller & Rincon-Camacho **2011**

Discrepancy principle: Wen & Chan **2012**

S-curve method: Kolehmainen, Lassas, Niinimäki & S **2012**

Dantzig estimation: Frick, Marnitz & Munk **2012**

Quasi-optimality principle and Hanke-Raus rules: Kindermann, Mutimbu & Resmerita **2013**

KKT system: Chen, Loli Piccolomini & Zama **2014**

Discrepancy principle: Toma, Sixou & Peyrin **2015**

Cross validation, Stein's unbiased risk estimates, L-curve method, ...

No single choice rule works perfectly for all applications. Therefore, it is good to have a collection of rules.

The continuous tomographic model needs to be approximated using a discrete model

Continuous model:

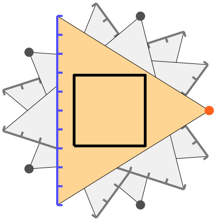

Discrete model:

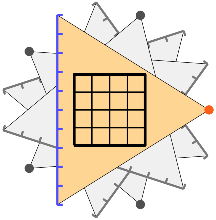

In this schematic setup we have 5 projection directions and a 10-pixel detector. Therefore, the number of data points is **50**.

The resolution of the discrete model can be freely chosen according to computational resources

Continuous model:

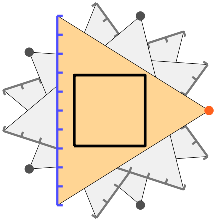

In this schematic setup we have 5 projection directions and a 10-pixel detector. Therefore, the number of data points is **50**.

The number of degrees of freedom in the three discrete models below are **16**, **64** and **256**, respectively.

Discrete models:

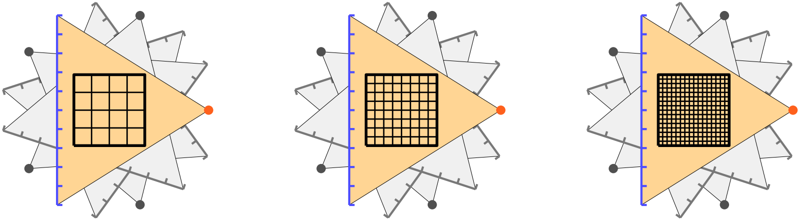

We define the total variation (TV) norm consistently for continuous and discrete cases

Continuous anisotropic TV norm for attenuation coefficient $f : \Omega \to \mathbb{R}$:

$$\int_\Omega \left(\left| \frac{\partial f}{\partial x_1} \right| + \left| \frac{\partial f}{\partial x_2} \right| \right) dx.$$

Discrete anisotropic TV norm for an image matrix of size $n \times n$:

$$\frac{1}{n} \sum \left| \mathbf{f}_\kappa - \mathbf{f}_{\kappa'} \right|,$$

where the sum is over horizontally and vertically neighboring pixel values $\mathbf{f}_\kappa$ and $\mathbf{f}_{\kappa'}$.

The above is based on this approximate two-dimensional computation:

$$\int_\Omega \left| \frac{f(x_1 + \frac{1}{n}, x_2) - f(x_1, x_2)}{1/n} \right| dx \approx (1/n)^2 \sum \left| \frac{\mathbf{f}_\kappa - \mathbf{f}_{\kappa'}}{1/n} \right|,$$

where the sum is over horizontally neighboring pixel values $\mathbf{f}_\kappa$ and $\mathbf{f}_{\kappa'}$.

Outline

We collected X-ray projection data of a walnut from 1200 directions

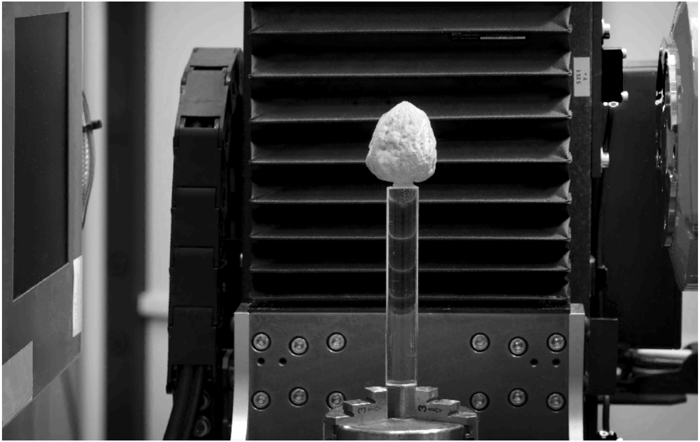
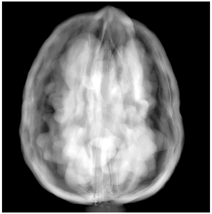
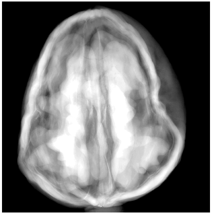

Laboratory and data collection by Keijo Hämäläinen and Aki Kallonen, University of Helsinki.

The data is openly available at http://fips.fi/dataset.php, thanks to Esa Niemi and Antti Kujanpää

Reconstructions of a 2D slice through the walnut using filtered back-projection (FBP)

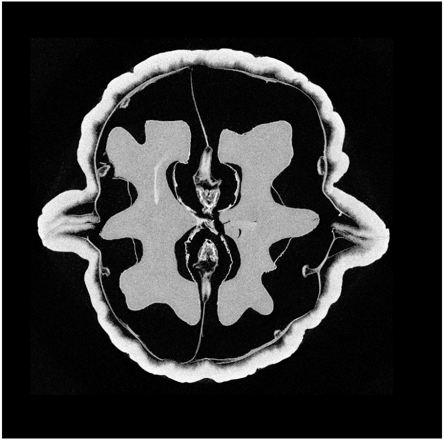

FBP with comprehensive data
(1200 projections)

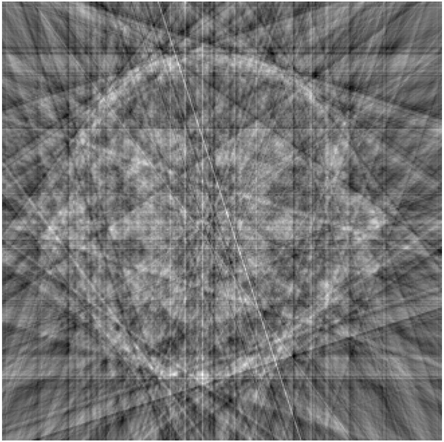

FBP with sparse data
(20 projections)

Low-noise TV reconstructions of a walnut using several regularization parameters

$\alpha = 0.001$

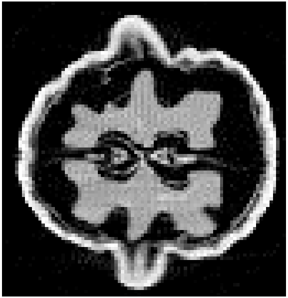

Too small α

$\alpha = 1$

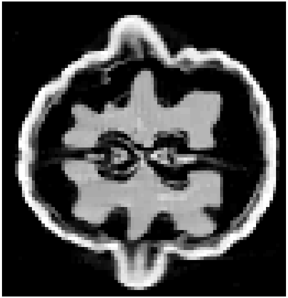

Just right α

$\alpha = 1000$

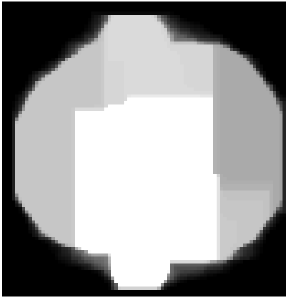

Too large α

Computations by Kati Niinimäki using a primal-dual interior point method.

Low-noise TV reconstructions of a walnut using several regularization parameters

$\alpha = 0.001$

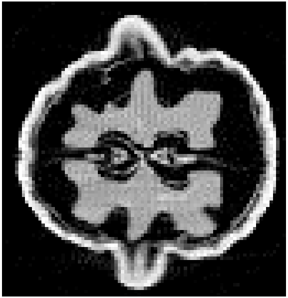

Too small α

$\alpha = 1$

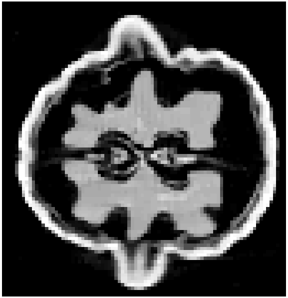

Just right α

$\alpha = 1000$

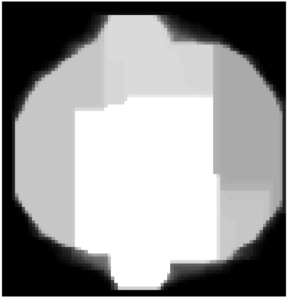

Too large α

What happens when we compare reconstructions at different resolutions?

Low-noise TV reconstructions of a walnut at many resolutions using $\alpha = 0.001$

128×128

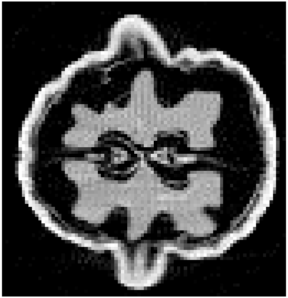

192×192

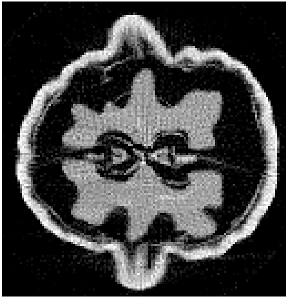

256×256

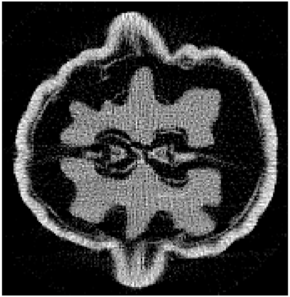

Low-noise TV reconstructions of a walnut at many resolutions using $\alpha = 1$

128×128

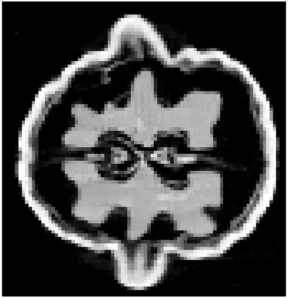

192×192

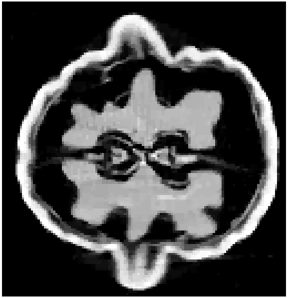

256×256

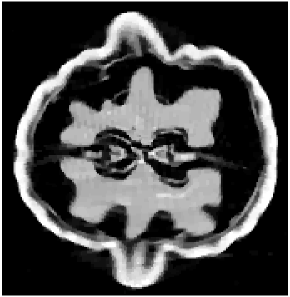

Low-noise TV reconstructions of a walnut at many resolutions using $\alpha = 1000$

128×128

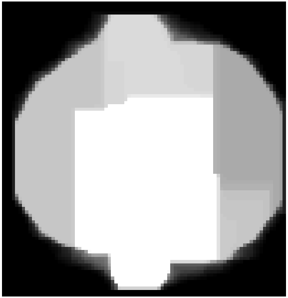

192×192

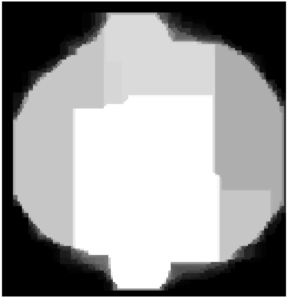

256×256

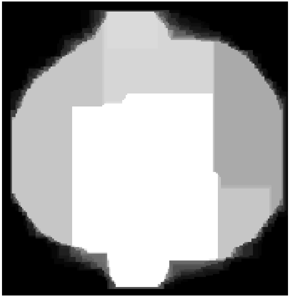

TV norms of low-noise reconstructions with various resolutions and parameters α

α	Resolution 128×128	192×192	256×256
10^{-4}	1.51	2.29	3.64
10^{-3}	1.51	2.29	3.46
10^{-2}	1.50	2.23	2.97
10^{-1}	1.43	1.85	1.93
10^{0}	1.08	1.11	1.11
10^{1}	0.78	0.78	0.77
10^{2}	0.48	0.48	0.48
10^{3}	0.12	0.12	0.12
10^{4}	0.04	0.04	0.04
10^{5}	0	0	0
10^{6}	0	0	0

TV norms of low-noise reconstructions with various resolutions and parameters α

α	Resolution 128×128	192×192	256×256
10^{-4}	1.51	2.29	3.64
10^{-3}	1.51	2.29	3.46
10^{-2}	1.50	2.23	2.97
10^{-1}	1.43	1.85	1.93
10^{0}	1.08	1.11	1.11
10^{1}	0.78	0.78	0.77
10^{2}	0.48	0.48	0.48
10^{3}	0.12	0.12	0.12
10^{4}	0.04	0.04	0.04
10^{5}	0	0	0
10^{6}	0	0	0

What happens when we add noise to the data?

5% noise TV reconstructions of a walnut at many resolutions using $\alpha = 0.001$

128×128

192×192

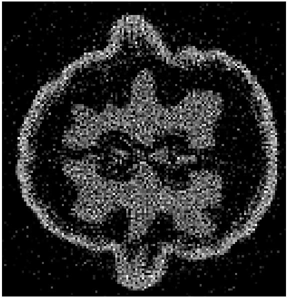

256×256

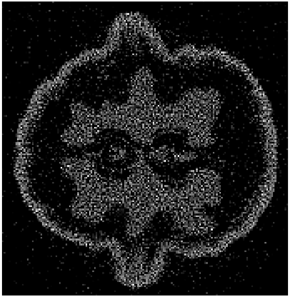

5% noise TV reconstructions of a walnut at many resolutions using $\alpha = 10$

128×128

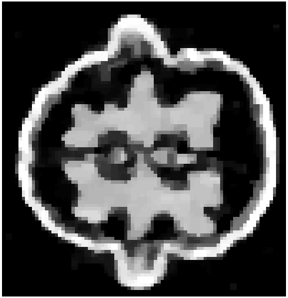

192×192

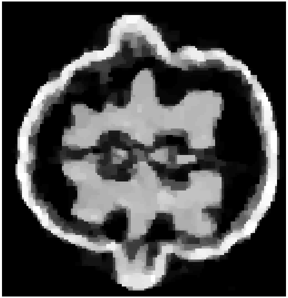

256×256

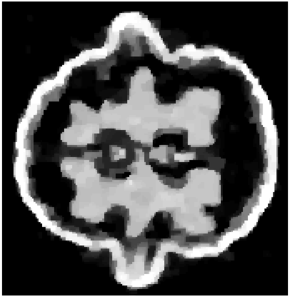

5% noise TV reconstructions of a walnut at many resolutions using $\alpha = 10000$

128×128

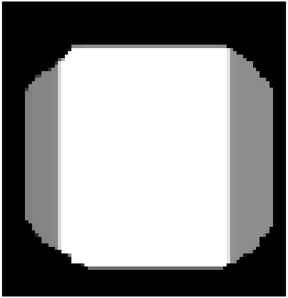

192×192

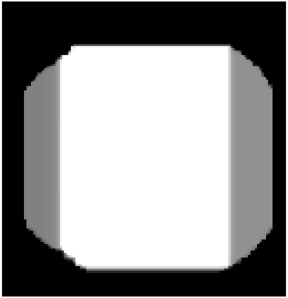

256×256

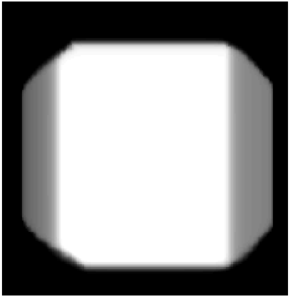

TV norms of reconstructions using various noise levels, resolutions and parameters α

	Low noise			5% noise		
α	128^2	192^2	256^2	128^2	192^2	256^2
10^{-4}	1.51	2.29	3.64	2.42	5.05	8.71
10^{-3}	1.51	2.29	3.46	2.43	5.05	8.59
10^{-2}	1.50	2.23	2.97	2.42	5.01	8.59
10^{-1}	1.43	1.85	1.93	2.37	4.83	8.16
10^{0}	1.08	1.11	1.11	1.99	3.50	5.12
10^{1}	0.78	0.78	0.77	0.86	0.86	0.88
10^{2}	0.48	0.48	0.48	0.48	0.48	0.48
10^{3}	0.12	0.12	0.12	0.12	0.12	0.12
10^{4}	0.04	0.04	0.04	0.04	0.04	0.04
10^{5}	0	0	0	0	0	0
10^{6}	0	0	0	0	0	0

[Niinimäki, Lassas, Hämäläinen, Kallonen, Kolehmainen, Niemi & S, SIAM Journal on Imaging Sciences 2016]

Outline

There are some related results in the literature

1992 **Vainikko**: *On the discretization and regularization of ill-posed problems with noncompact operators*

We use geometric arguments similar to those here:
1995 **Chambolle**: *Image Segmentation by Variational Methods: Mumford and Shah Functional and the Discrete Approximations.*

These works consider TV functionals and Γ-convergence when discretization is refined, but without a measurement operator:
2009 **Chambolle, Giacomini & Lussardi**
2012 **Gennip & Bertozzi**
2013 **Bellettini, Chambolle & Goldman**
2013 **Trillos & Slepčev**

This paper achieves a result analogous with ours, using wavelet frames in the finite-dimensional functionals:
2012 **Cai, Dong, Osher & Shen**

Assumptions on the linear forward map $\mathcal{A}$

Assume either **(A)** or **(B)** about the linear operator $\mathcal{A}$:

(A) $\mathcal{A} : L^2(D) \to L^2(\Omega)$ is compact and $\mathcal{A} : L^1(D) \to \mathcal{D}'(\Omega)$ is continuous with some open and bounded set $\Omega \subset \mathbb{R}^2$.
This covers the case of classical Radon transform with image domain D and sinogram domain Ω. We denote the set of distributions by $D'(\Omega)$.

(B) $\mathcal{A} : L^1(D) \to \mathbb{R}^M$ is bounded.
This covers the practically important discrete pencil beam model of tomographic measurements.

Definition of discrete and continuous regularization functionals

Let D be the square $[0,1]^2 \subset \mathbb{R}^2$. Use anisotropic $BV(D)$ norm

$$\|u\|_{BV} = \|u\|_{L^1} + V(u) = \|u\|_{L^1} + \int_D \left(\left| \frac{\partial u(x)}{\partial x_1} \right| + \left| \frac{\partial u(x)}{\partial x_2} \right| \right) dx.$$

Define $S_\infty : BV(D) \to \mathbb{R}$ and $S_j : BV(D) \to \mathbb{R} \cup \{\infty\}$ by

$$S_\infty(u) = \|\mathcal{A}u - m\|^2_{L^2(\Omega)} + \alpha_1 \|u\|_{L^1(D)} + \alpha V(u)$$

with positive regularization parameters $\alpha_1 > 0$ and $\alpha > 0$, and

$$S_j(u) = \begin{cases} S_\infty(u), & \text{for } u \in \mathrm{Range}(T_j), \\ \infty, & \text{for } u \notin \mathrm{Range}(T_j). \end{cases}$$

Linear operator T_j projects to functions that are piecewise constant on a regular $2^j \times 2^j$ square pixel grid.

Our main theorem ensures the convergence of regularized solutions as resolution grows

- There exists a minimizer $\widetilde{u}_j \in \arg\min(S_j)$ for all $j = 1, 2, 3, \ldots$
- There exists a minimizer $\widetilde{u}_\infty \in \arg\min(S_\infty)$.
- Any sequence $\widetilde{u}_j \in \arg\min(S_j)$ of minimizers has a subsequence $\widetilde{u}_{j(\ell)}$ that converges weakly in $BV(D)$ to some limit $w \in BV(D)$. Furthermore, $\lim_{\ell\to\infty} V(\widetilde{u}_{j(\ell)}) = V(w)$.
- The limit w is a minimizer: $w \in \arg\min(S_\infty)$.

[Niinimäki, Lassas, Hämäläinen, Kallonen, Kolehmainen, Niemi & S, SIAM Journal on Imaging Sciences 2016]

How to prove the main theorem?

The proof is an analysis of Γ-convergence of functionals S_j to S_∞. However, the choice of topologies is very delicate. For details, see http://arxiv.org/abs/0902.2313v1.

Note: related Γ-convergence results of TV functionals are given in [Chambolle, Giacomini and Lussardi 2009], but they do not consider measurement operators.

This approximation lemma serves as the foundation of the proof:

Lemma. For all $u \in BV(D)$ and $\varepsilon > 0$ there exists $j > 0$ and a function u', piecewise constant in the dyadic $2^j \times 2^j$ grid, such that

$$\|u - u'\|_{L^1(D)} + |V(u) - V(u')| < \varepsilon.$$

Recall that

$$V(u) = \int_D \Big(\Big|\frac{\partial u(x)}{\partial x_1}\Big| + \Big|\frac{\partial u(x)}{\partial x_2}\Big| \Big) dx.$$

We need to move from triangulation-based to pixel-based approximation

[Bělík and Luskin 2003]: the desired inequality holds with PW constant functions in a fine triangularization.

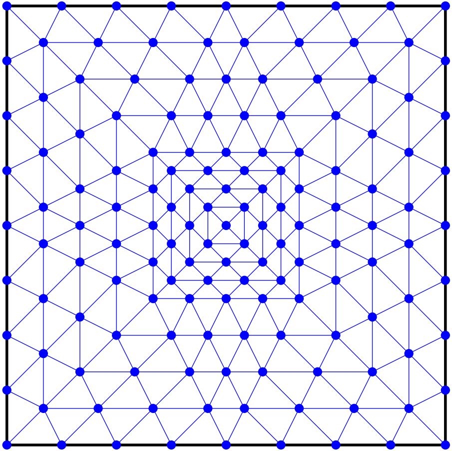

However, we need to work with dyadic $2^j \times 2^j$ pixel grids.

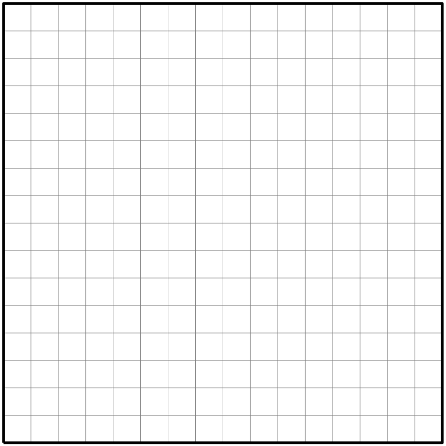

We surround any triangle vertex (blue dot) with a “pixel cluster” neighborhood (gray box)

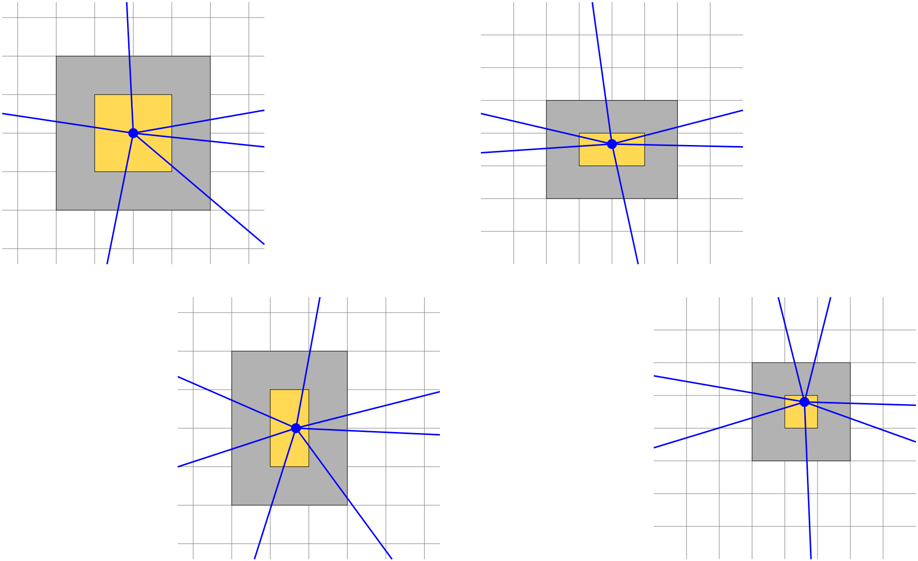

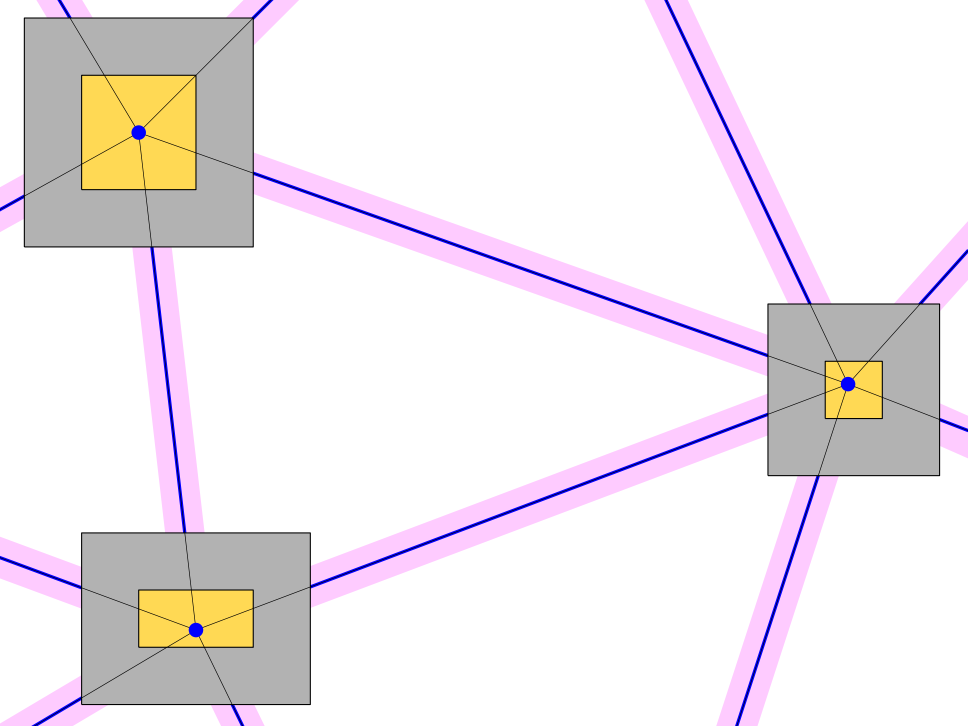

Refine the grid outside clusters so that pixel-wise polygonal chains (on pink) connect the clusters

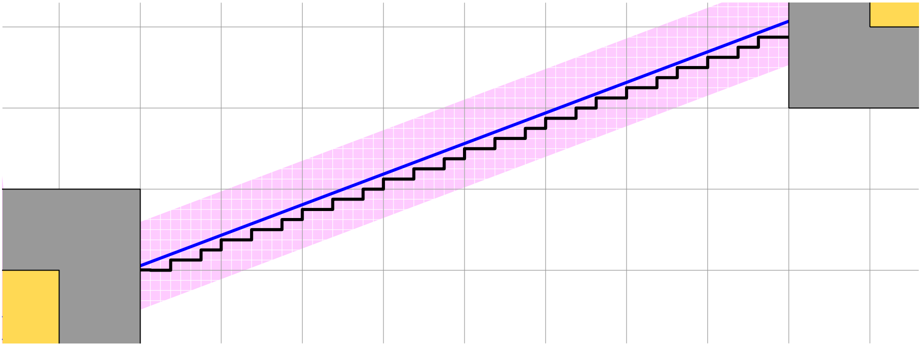

Using the anisotropic BV norm reduces the approximation to estimating small intervals

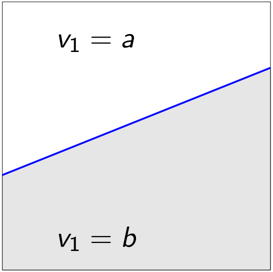

The difference between the BV norms of the piecewise constant functions v_1 and v_2 comes entirely from jumps over the two red vertical intervals below.

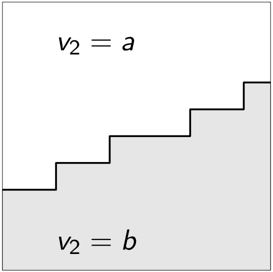

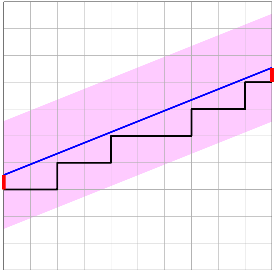

What can we say about the proposed method?

Benefits of our multiresolution TV parameter choice method:

- simple definition,
- easy implementation, and
- no need of *a priori* information about the noise amplitude.

Also, it seems to perform well for real tomographic data.

Downside: several reconstructions need to be computed. Also, it is still unclear why the method works so nicely: if there is convergence for any α in theory, what is the instability we are observing?

The method can be tried out with 3D tomography (it works!) and with other inverse problems and regularizers.

Outline

We study a tomographic imaging modality based on multiple source-detector pairs

Place several X-ray sources and detectors in fixed positions in 3D. The detectors should have a high framerate relative to the movement of the object under imaging.

Reconstructing the 3D structure at all frames leads to 4D tomography.

Applications include
cardiac imaging,
angiography,
biotechnology research,
veterinary medicine,
nondestructive testing.

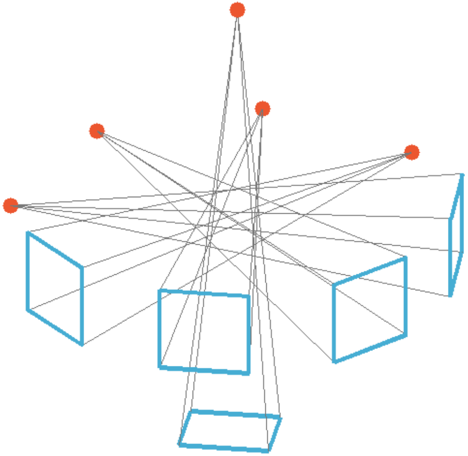

Dynamic Spatial Reconstructor

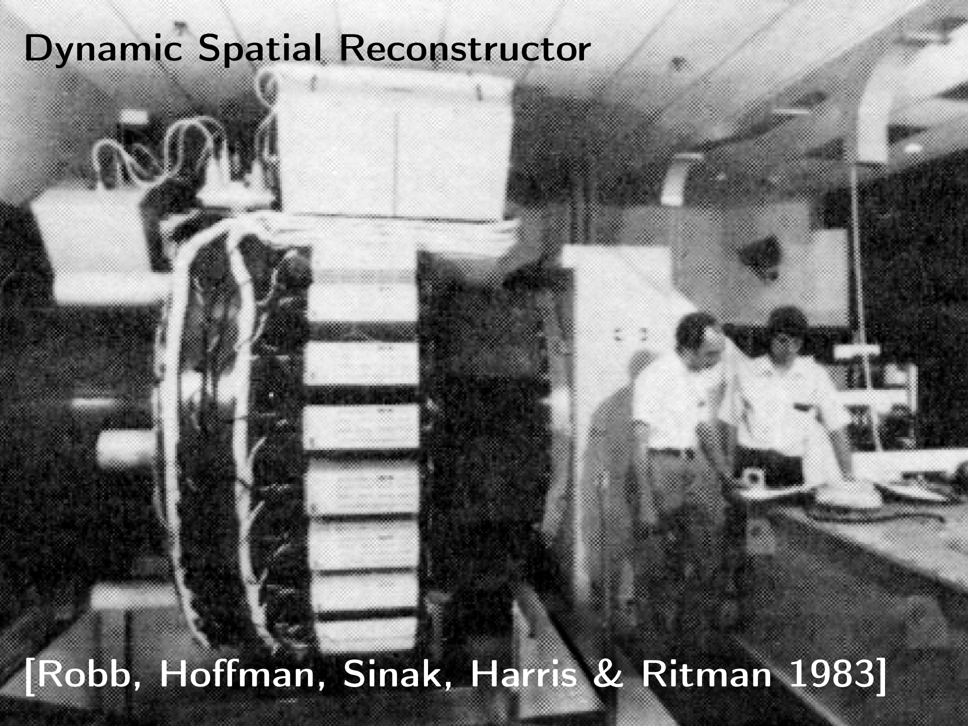

[Robb, Hoffman, Sinak, Harris & Ritman 1983]

One potential benefit of this imaging modality is three-dimensional angiography

This is regular two-dimensional angiography.

Video by Dr. Magda Bayoumi, downloaded from *Dailymotion*

Very brief overview of multi-source tomographic studies, all based on FBP-type algorithms

1980 **Berninger & Redington**: Multiple purpose high speed tomographic x-ray scanner (patent)

1983 **Robb, Hoffman, Sinak, Harris & Ritman**: High-speed three-dimensional x-ray computed tomography: The dynamic spatial reconstructor

1993 **Stiel, Stiel, Klotz & Nienaber**: Digital flashing tomosynthesis: a promising technique for angiocardiographic screening

2001 **Liu, Liu, Wang & Wang**: Half-scan cone-beam CT fluoroscopy with multiple x-ray sources

Static multi-source arrangements have received very little attention in the literature. Filtered back-projection type methods are not well-suited for the resulting sparse datasets.

Reconstruction methods for dynamic tomography

- **1997** **Baroudi & Somersalo**: Gas temperature mapping using impedance tomography
- **2002** **Lu & Mackie**: Tomographic motion detection and correction directly in sinogram space
- **2003** **Bonnet *et al.***: Dynamic X-Ray Computed Tomography
- **2004** **Roux *et al.***: Exact reconstruction in 2D dynamic CT: compensation of time-dependent affine deformations
- **2006** **Kindermann & Leitão**: On regularization methods for inverse problems of dynamic type
- **2010** **Katsevich**: An accurate approximate algorithm for motion compensation in two-dimensional tomography
- **2014** **Hahn**: Reconstruction of dynamic objects with affine deformations in computerized tomography
- **2015** **Hahn**: Dynamic linear inverse problems with moderate movements of the object: Ill-posedness and regularization

X-ray sources and detectors are expensive, and surrently we have only one of each.

How to use one X-ray source and one detector to create a multi-source type dataset?

Consider a simple multi-source measurement:

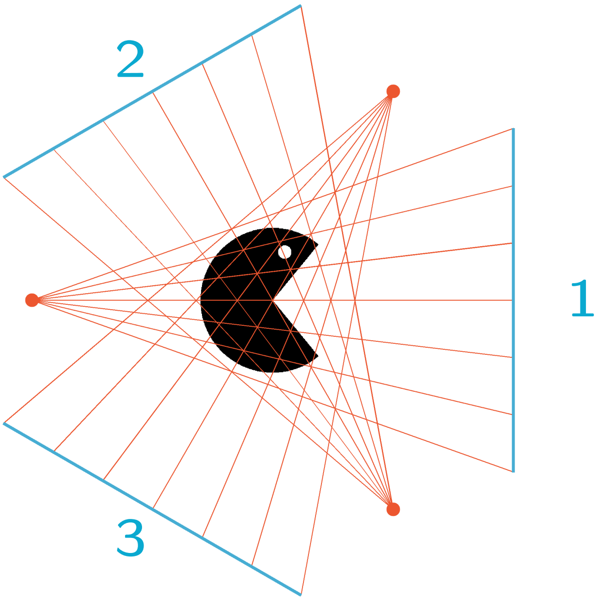

$t = 1$

Consider a simple multi-source measurement:

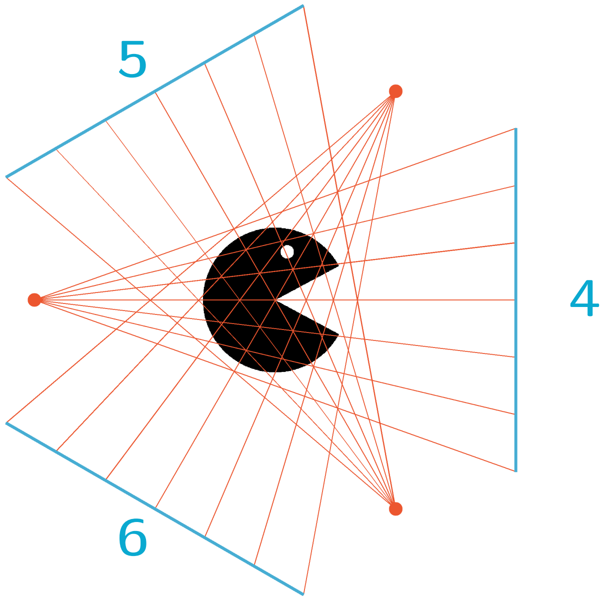

$t = 2$

Consider a simple multi-source measurement:

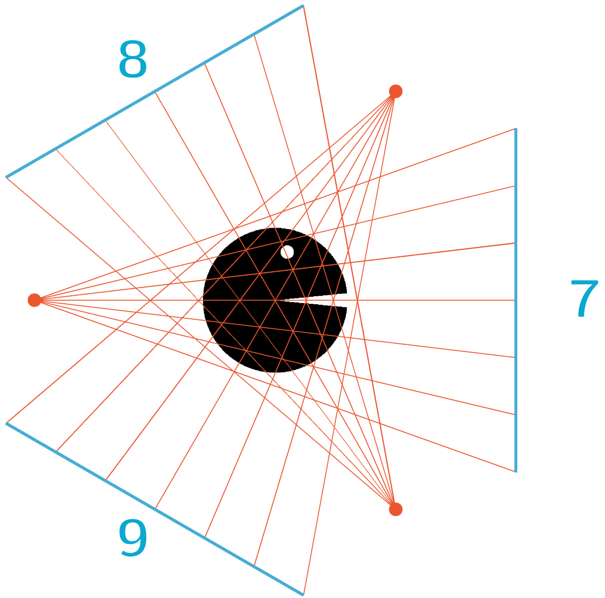

$t = 3$

We can collect the same dataset by rotating, if the object stays stationary during rotation:

$t = 1$

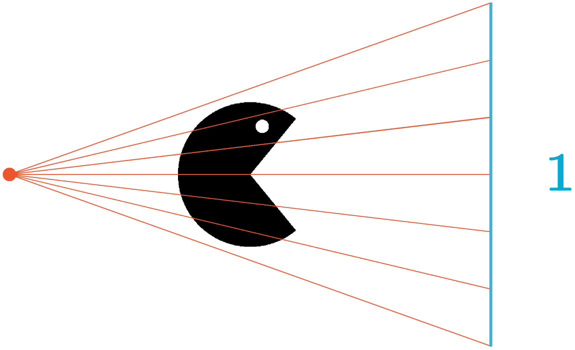

We can collect the same dataset by rotating, if the object stays stationary during rotation:

$t = 1$

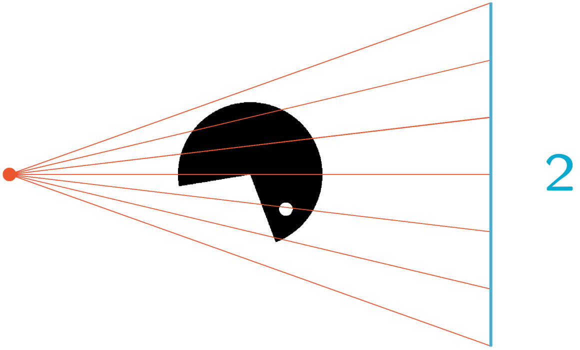

We can collect the same dataset by rotating, if the object stays stationary during rotation:

$t = 1$

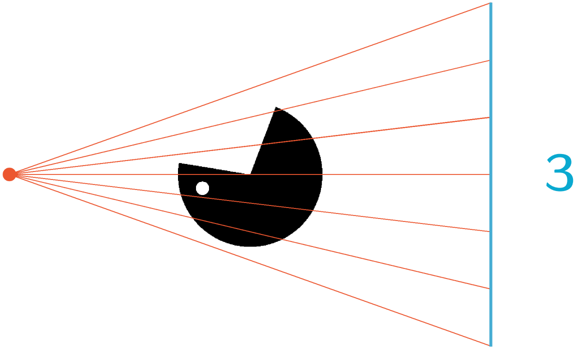

We can collect the same dataset by rotating, if the object stays stationary during rotation:

$t = 2$

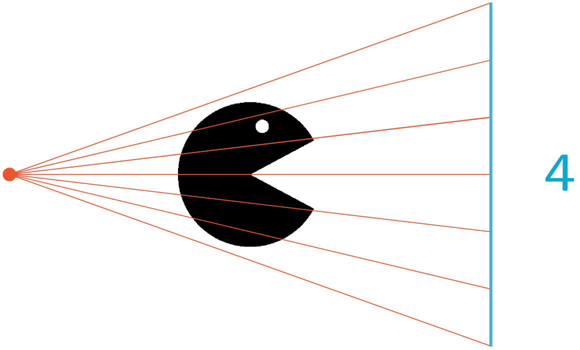

We can collect the same dataset by rotating, if the object stays stationary during rotation:

$t = 2$

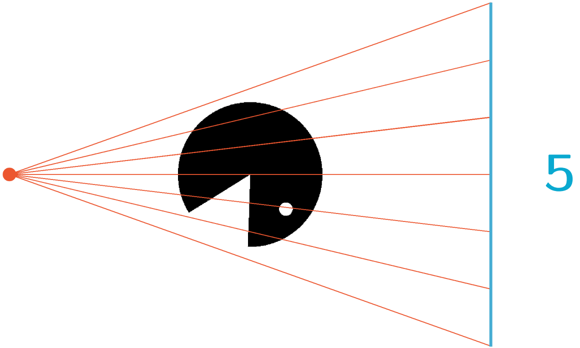

We can collect the same dataset by rotating, if the object stays stationary during rotation:

$t = 2$

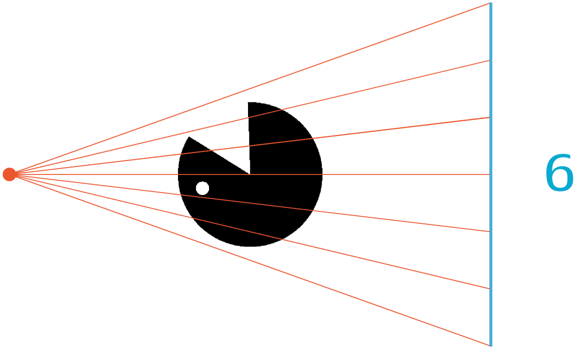

We can collect the same dataset by rotating, if the object stays stationary during rotation:

$t = 3$

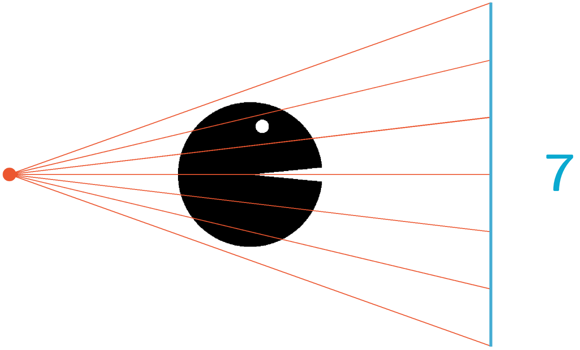

We can collect the same dataset by rotating, if the object stays stationary during rotation:

$t = 3$

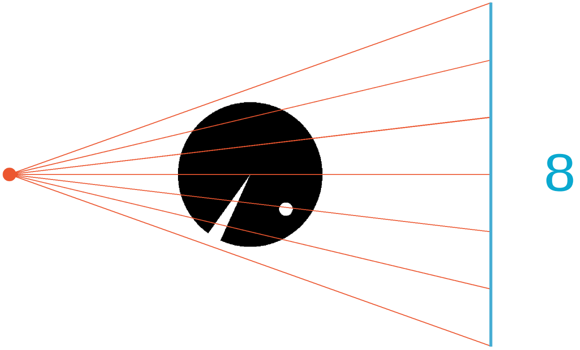

We can collect the same dataset by rotating, if the object stays stationary during rotation:

$t = 3$

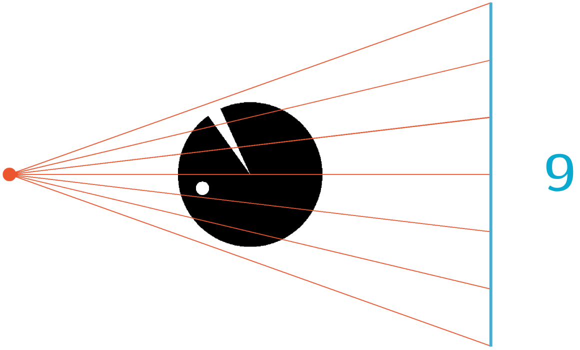

Outline

This is a joint work with

Keijo Hämäläinen, University of Helsinki, Finland

Lauri Harhanen, KaVo Kerr Group

Aki Kallonen, University of Helsinki, Finland

Ville Kolehmainen, University of Eastern Finland

Matti Lassas, University of Helsinki, Finland

Esa Niemi, University of Helsinki, Finland

The level set method can be used to model mud

The level set method [Osher, Sethian] parametrizes curves and surfaces in a flexible way

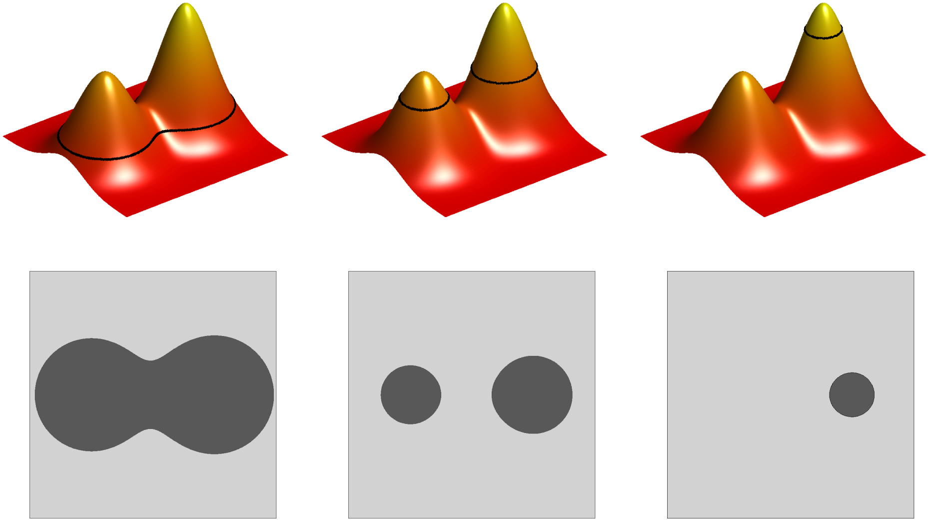

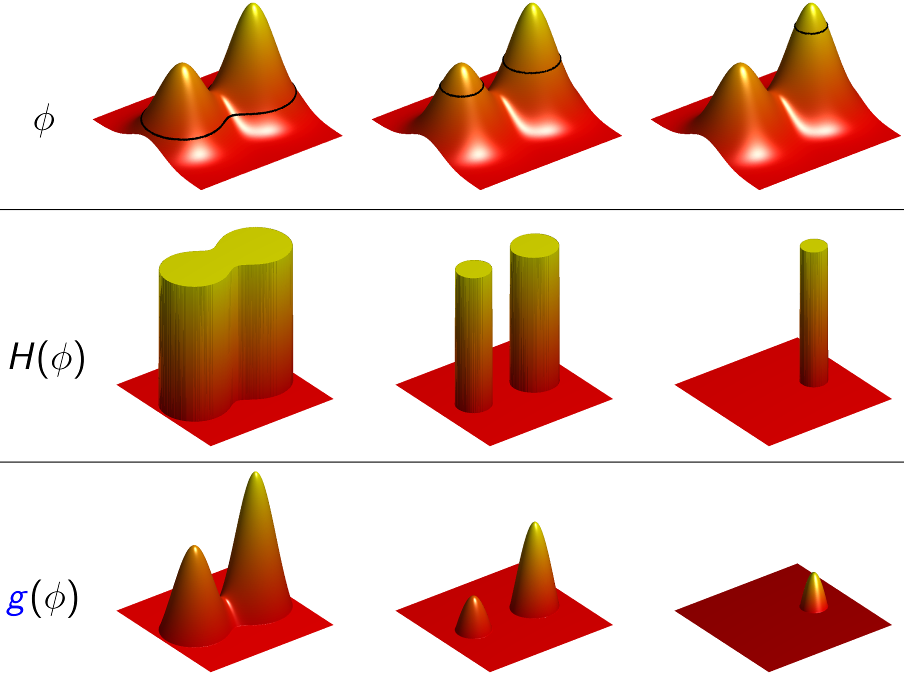
ϕ
$H(\phi)$
$g(\phi)$

A generalization of the classical level set method was introduced in [Kolehmainen, Lassas & S 2008]

We model the X-ray attenuation function as $g(\Phi(x,y))$, where

$$g(\tau) = \begin{cases} \tau, & \text{if } \tau \geq 0 \\ 0, & \text{if } \tau < 0. \end{cases}$$

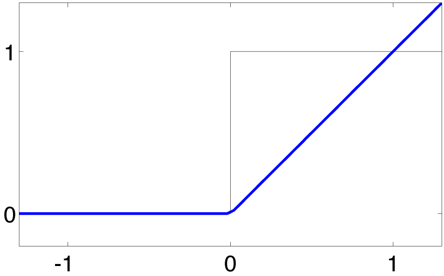

The smooth level set function $\Phi(x,y) := \lim_{s\to\infty} \phi(x,y,s)$ is the large-time limit of the solution of the evolution equation

$$\begin{cases} \phi_s = -A^*(A(g(\phi)) - m) + \beta\Delta\phi, \\ (\nu \cdot \nabla - r)\phi|_{\partial\Omega} = 0, \end{cases}$$

with a suitable initial condition. Here $\beta > 0$, $r \geq 0$, A^* denotes the transpose of A, and $\Delta\phi = \phi_{xx} + \phi_{yy}$.

The generalized level set method works nicely for stationary limited-angle 2D tomography

Ground truth

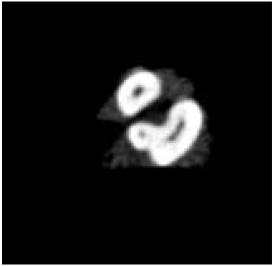

Full angle

Back-projection

Limited angle

Level set method

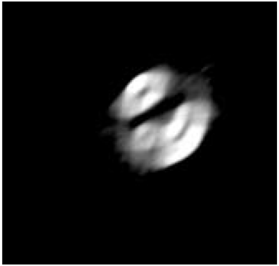

Limited angle

Images from [Kolehmainen, Lassas & S **2008**]. However, see also [Niemi, Lassas, Kallonen, Harhanen, Hämäläinen and S **2015**]

We deal with the dynamic case by considering the moving target in spacetime

We write a higher-order level set method in (2+1)D spacetime for the dynamic case

The 2D static case:

We model the X-ray attenuation as $g(\phi(x,y))$. The level set function ϕ belongs to $H^1(\Omega)$ and is defined as the minimizer of

$$\|\mathcal{A}g(\phi) - m\|_{L^2}^2 + \alpha\|\nabla\phi\|_{L^2}^2,$$

where $\nabla\phi = [\phi_x, \phi_y]^T$.

[Kolehmainen, Lassas & S **2008**]

The (2+1)D dynamic case:

We model the X-ray attenuation as $g(\Phi(x,y,t))$. The level set function ϕ belongs to $H^2(\Omega \times [0,T])$ and is defined as the minimizer of

$$\|\mathcal{A}g(\phi) - m\|_{L^2}^2 + \alpha\|\nabla\phi\|_{L^2}^2 +$$
$$+\alpha(\|\partial_x^2\phi\|_{L^2}^2 + \|\partial_y^2\phi\|_{L^2}^2 + \|\partial_t^2\phi\|_{L^2}^2),$$

where $\nabla\phi = [\phi_x, \phi_y, \phi_t]^T$.

[Niemi, Lassas, Kallonen, Harhanen, Hämäläinen and S **2015**]

There exists at least one minimizer for our generalized level set functional

Theorem: Let $\mathcal{A}$ be an operator modeling 2D Radon transforms measured at several times. If $\alpha > 0$ satisfies an upper bound involving the signal-to-noise ratio, then the nonlinear functional

$$F_n(\phi) := \frac{1}{2}\|\mathcal{A}g(\phi) - m\|_2^2 + \frac{\alpha}{2}\sum_{1\leq|\beta|\leq n}\|D^\beta\phi\|_2^2$$

has a **global minimizer**. The minimizer is unique for $n = 1$.

We model the X-ray attenuation function as $g(\Phi(x, y))$, where

$$g(\tau) = \begin{cases} \tau, & \text{if } \tau \geq 0 \\ 0, & \text{if } \tau < 0. \end{cases}$$

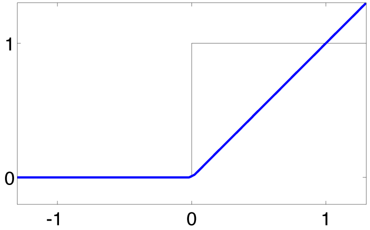

[Niemi, Lassas, Kallonen, Harhanen, Hämäläinen and S **2015**]

Numerical minimization in the case $n = 2$

We smooth out the nondifferentiability of the objective functional by replacing $g : \mathbb{R} \to \mathbb{R}$ by the differentiable approximation

$$g_\delta(\tau) = \begin{cases} \sqrt{\tau^2 + \delta^2} - \delta, & \text{if } \tau > 0, \\ 0, & \text{if } \tau \leq 0, \end{cases}$$

where $\delta > 0$ is small.

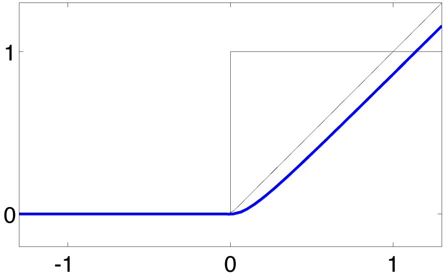

Now we can use a gradient-based optimization method for computing the minimizer of

$$\|\mathcal{A} g_\delta(\phi) - m\|_{L^2}^2 + \alpha \|\nabla \phi\|_{L^2}^2 +$$
$$+\alpha(\|\partial_x^2 \phi\|_{L^2}^2 + \|\partial_y^2 \phi\|_{L^2}^2 + \|\partial_t^2 \phi\|_{L^2}^2).$$

Two simulated examples, based on only seven (7) projection directions:

Imaging geometry:

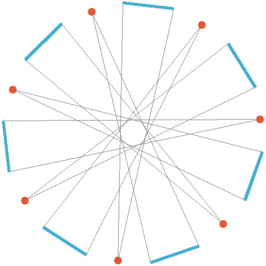

Spacetime phantoms:

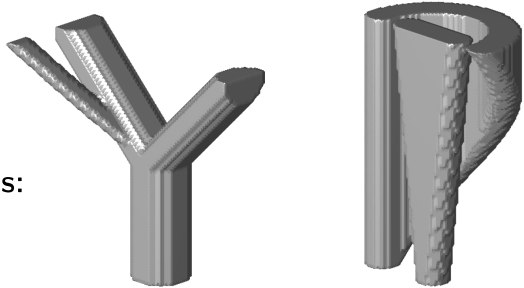

Original — Level set $n = 1$ — Level set $n = 2$ — Tikhonov 2D, ≥ 0 — TV 2D, ≥ 0

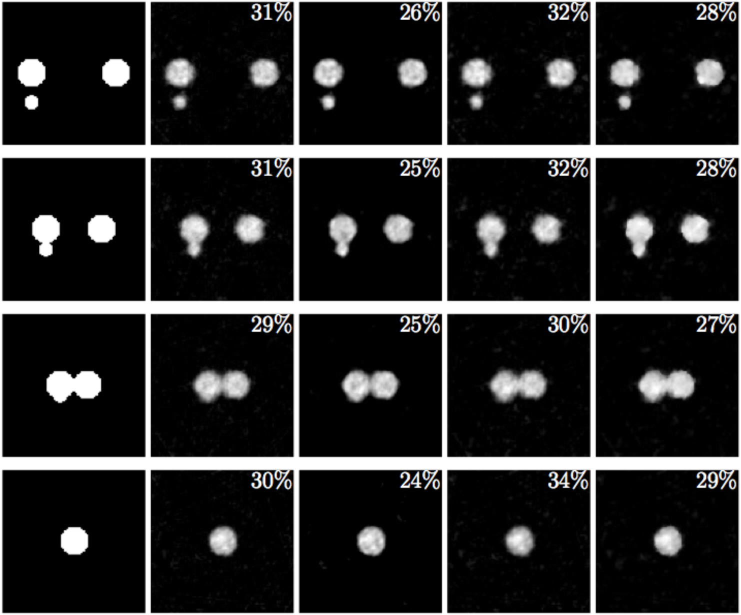

Level set reconstruction in spacetime

Original phantom

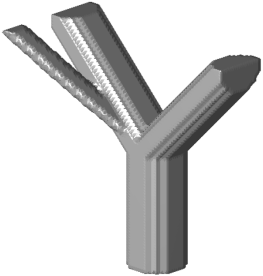

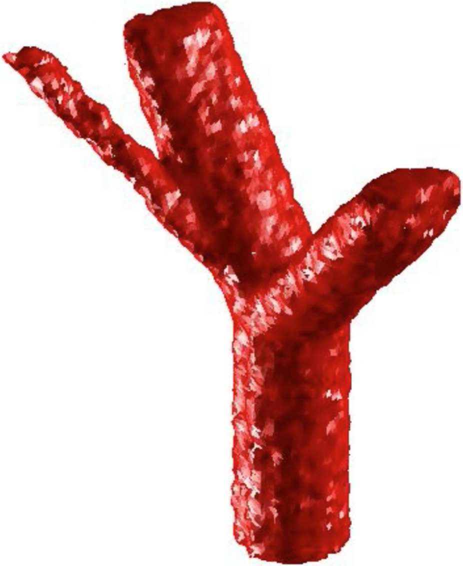

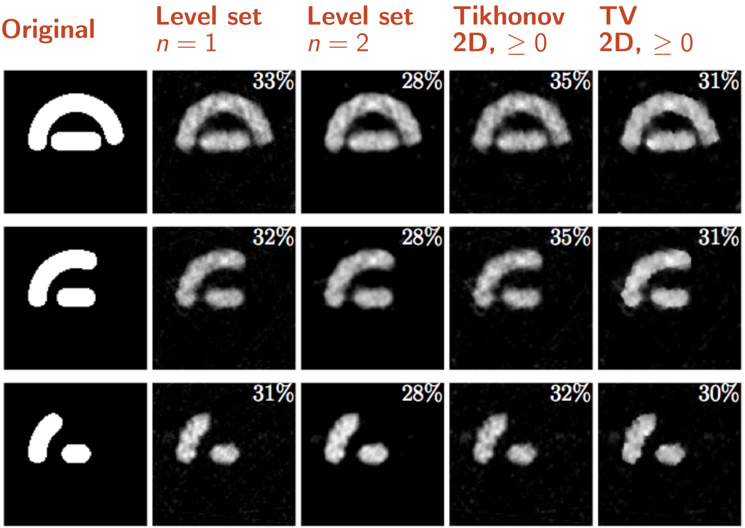

[Niemi, Lassas, Kallonen, Harhanen, Hämäläinen and S **2015**]

Level set reconstruction in spacetime

Original phantom

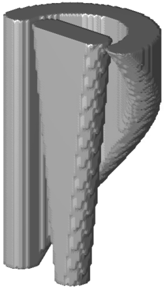

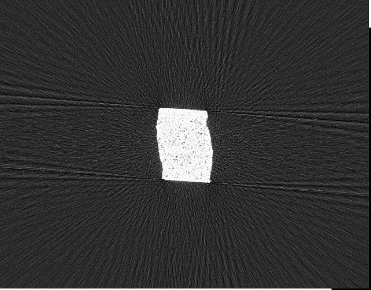

FBP reconstruction
from **120 projections**

$t = 1$

Tomographic data:
Keijo Hämäläinen
Aki Kallonen
Reconstruction:
Esa Niemi

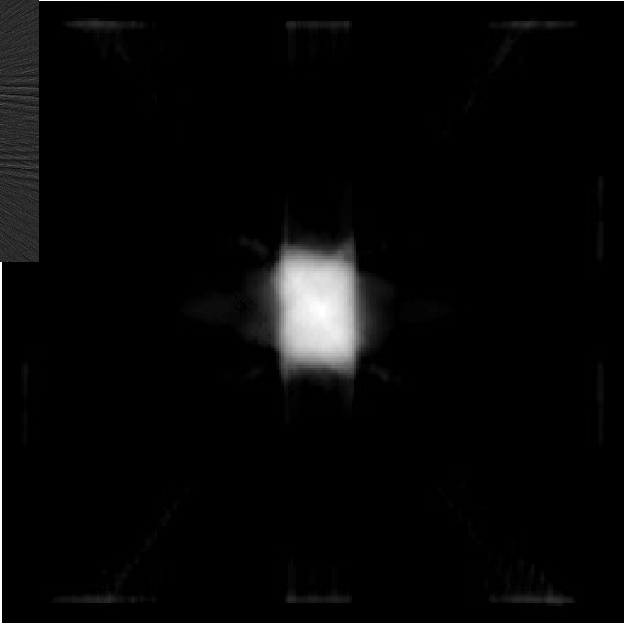

Level set ($n = 2$) reconstruction from **10 projections**

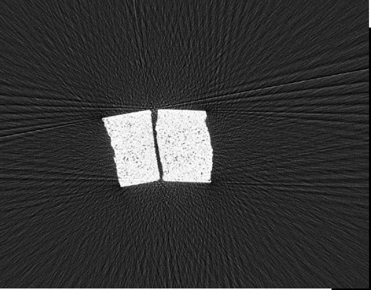

FBP reconstruction
from **120 projections**

$t = 2$

Tomographic data:
Keijo Hämäläinen
Aki Kallonen
Reconstruction:
Esa Niemi

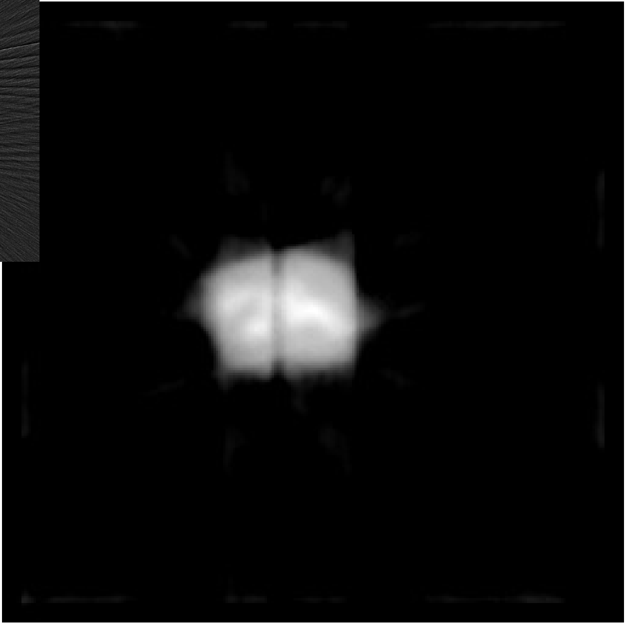

Level set ($n = 2$) reconstruction from **10 projections**

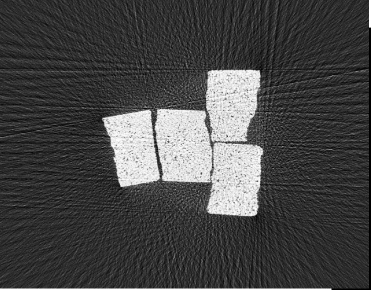

FBP reconstruction
from **120 projections**

$t = 3$

Tomographic data:
Keijo Hämäläinen
Aki Kallonen
Reconstruction:
Esa Niemi

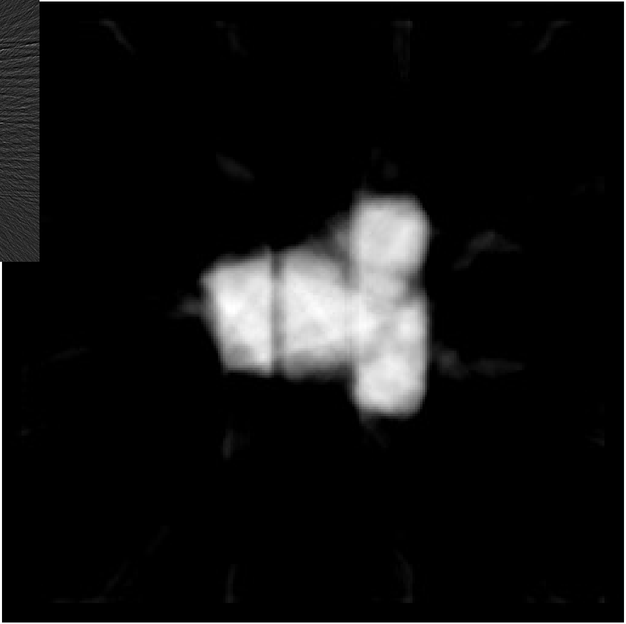

Level set ($n = 2$) reconstruction from **10 projections**

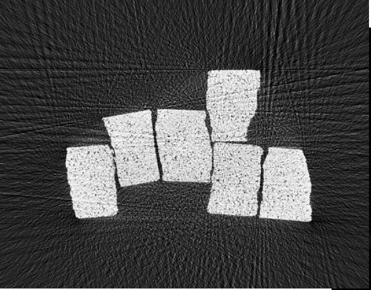

FBP reconstruction
from **120 projections**

$t = 4$

Tomographic data:
Keijo Hämäläinen
Aki Kallonen
Reconstruction:
Esa Niemi

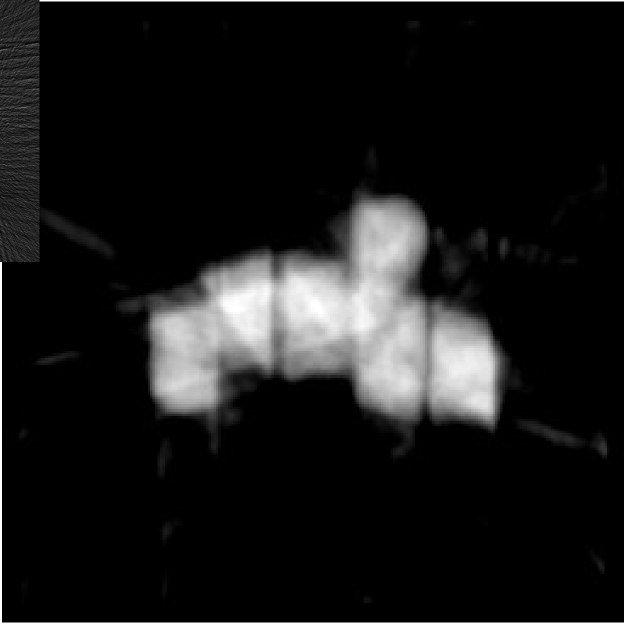

Level set ($n = 2$) reconstruction from **10 projections**

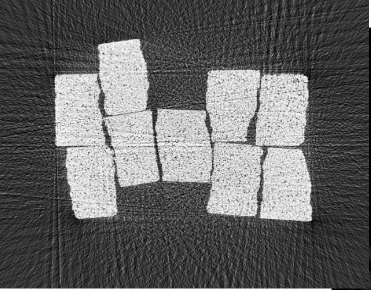

FBP reconstruction from **120 projections**

$t = 5$

Tomographic data:
Keijo Hämäläinen
Aki Kallonen
Reconstruction:
Esa Niemi

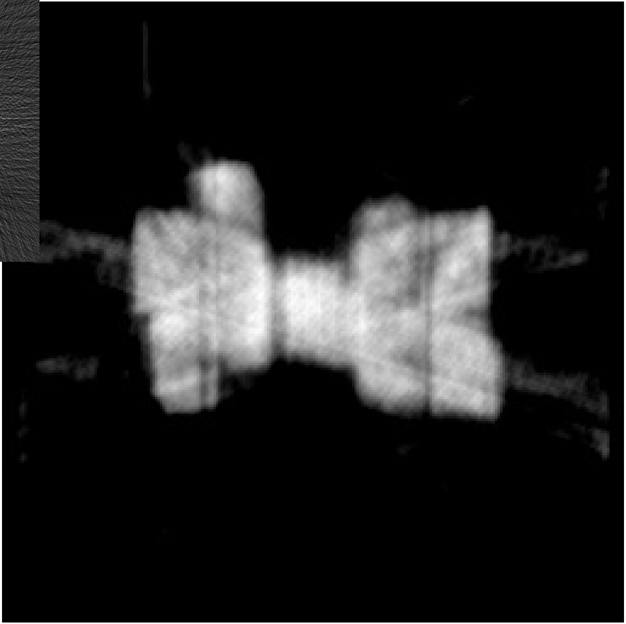

Level set ($n = 2$) reconstruction from **10 projections**

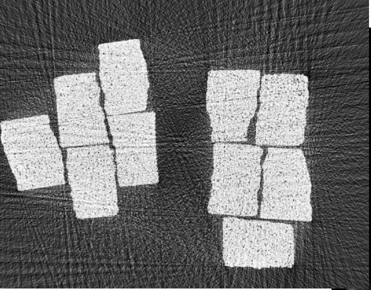

FBP reconstruction
from **120 projections**

$t = 6$

Tomographic data:
Keijo Hämäläinen
Aki Kallonen
Reconstruction:
Esa Niemi

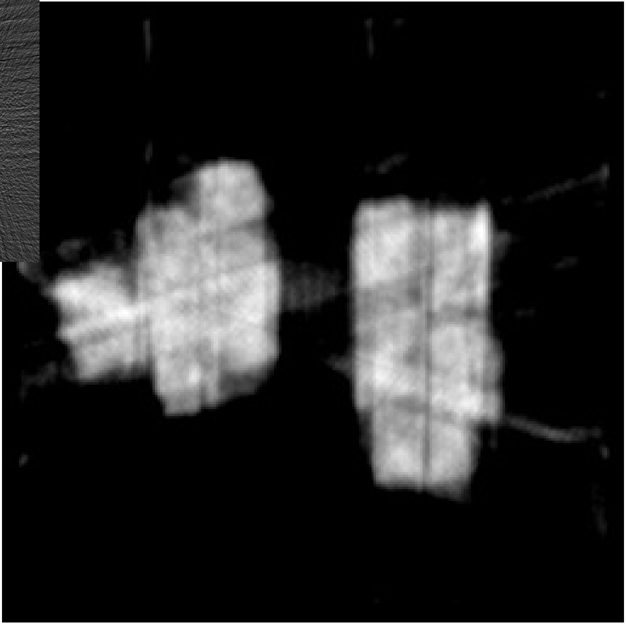

Level set ($n = 2$) reconstruction from **10 projections**

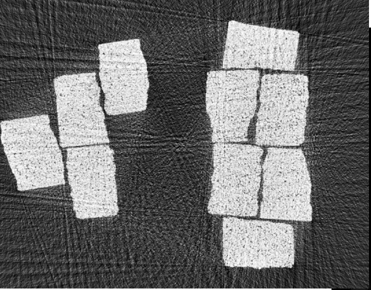

FBP reconstruction
from **120 projections**

$t = 7$

Tomographic data:
Keijo Hämäläinen
Aki Kallonen
Reconstruction:
Esa Niemi

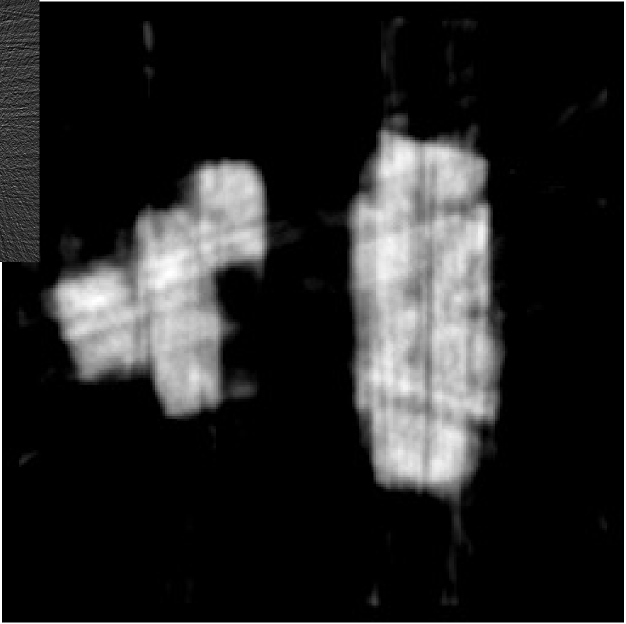

Level set ($n = 2$) reconstruction from **10 projections**

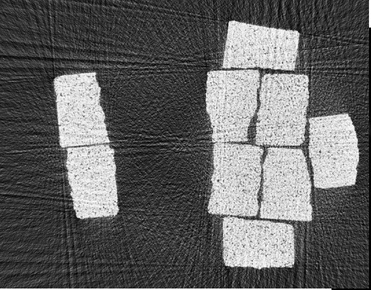

FBP reconstruction
from **120 projections**

$t = 8$

Tomographic data:
Keijo Hämäläinen
Aki Kallonen
Reconstruction:
Esa Niemi

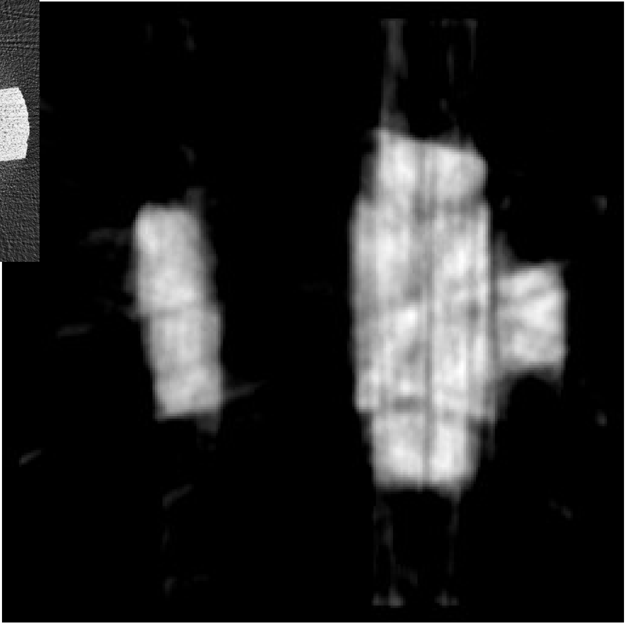

Level set ($n = 2$) reconstruction from **10 projections**

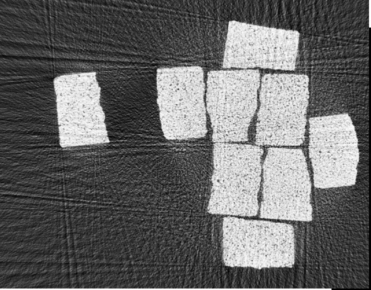

FBP reconstruction
from **120 projections**

$t = 9$

Tomographic data:
Keijo Hämäläinen
Aki Kallonen
Reconstruction:
Esa Niemi

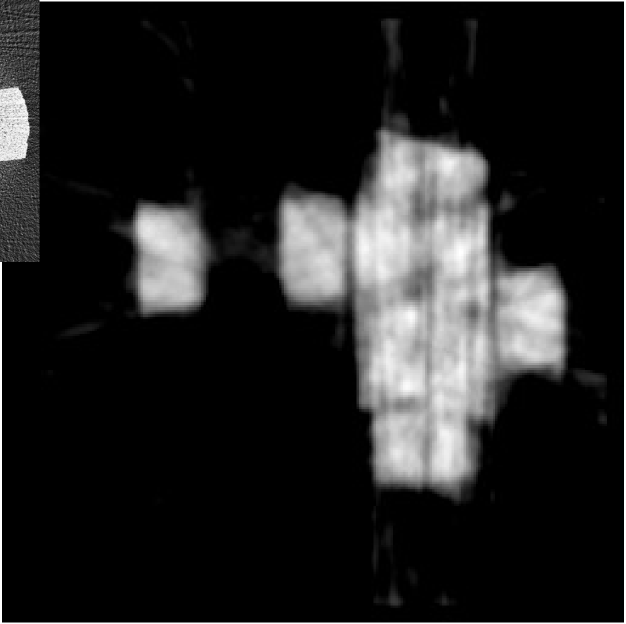

Level set ($n = 2$) reconstruction from **10 projections**

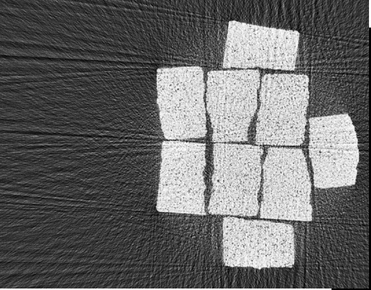

FBP reconstruction
from **120 projections**

$t = 10$

Tomographic data:
Keijo Hämäläinen
Aki Kallonen
Reconstruction:
Esa Niemi

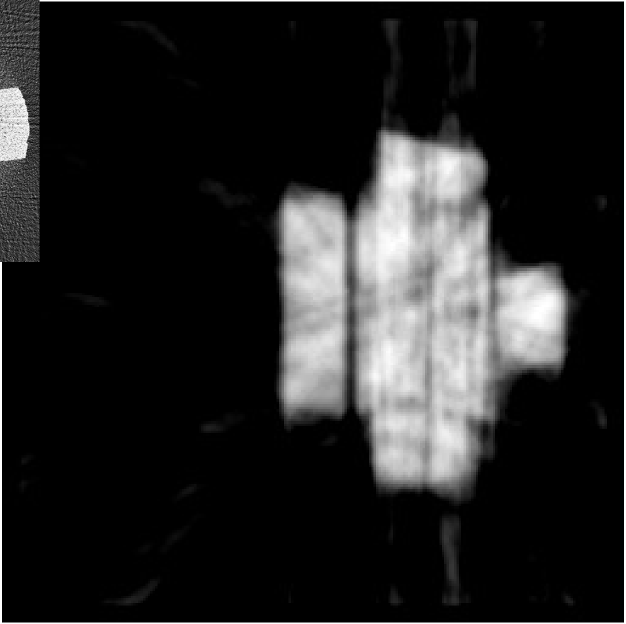

Level set ($n = 2$) reconstruction from **10 projections**

This is a movie showing the recovered level set in (2+1) dimensional spacetime

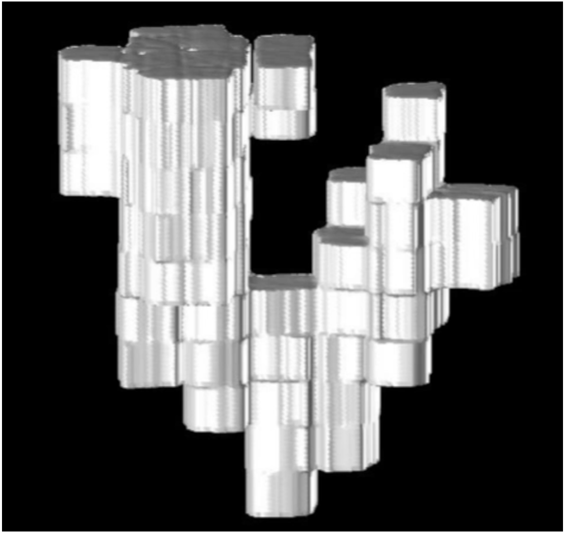

Computation and visualization by Esa Niemi

Outline

We consider (2+1)-dimensional spacetime and use 3-D shearlets to represent functions

The reconstruction is based on promoting shearlet sparsity using an ADMM optimization method.

[Bubba, März, Purisha, Lassas and S 2017]

Outline

The optical flow constraint

Assuming a constant image intensity of $f(x,t)$ along a trajectory $x(t)$ with a vector field $\frac{dx}{dt} = \boldsymbol{v}(x,t)$, we get by using the chain-rule

$$0 = \frac{df}{dt} = \frac{\partial f}{\partial t} + \sum_{i=1}^{2} \frac{\partial f}{\partial x_i}\frac{dx_i}{dt} = \partial_t f + \nabla f \cdot \boldsymbol{v}.$$

In short, the optical flow constraint is given by

$$\partial_t f + \nabla f \cdot \boldsymbol{v} = 0.$$

Optical flow functional

We have one equation for the flow field $\boldsymbol{v} = (v^1, v^2)^T$ and hence the problem is underdetermined.

To obtain an approximation we are minimizing

$$J_{\text{flow}}(f, \boldsymbol{v}) = \|\partial_t f + \nabla f \cdot \boldsymbol{v}\|_1 + \beta \sum_{i=1}^{2} \|v^i\|_{TV}.$$

The L^1-norm is more robust with respect to outliers for this model. [Zach, Pock, and Bischof, 2007]

An alternating algorithm for optical flow regularization for dynamic tomography

The joint model can be transformed into an iterative two-step method. Given $\boldsymbol{v}^k$ we compute

$$f^{k+1} = \arg\min_{f} \int_0^T \frac{1}{p} \|\mathcal{A}f - m\|_p^p + \alpha \|f\|_{TV} + \gamma \left\|\partial_t f + \nabla f \cdot \boldsymbol{v}^k\right\|_1 dt$$

$$\boldsymbol{v}^{k+1} = \arg\min_{\boldsymbol{v}} \int_0^T \left\|\partial_t f^{k+1} + \nabla f^{k+1} \cdot \boldsymbol{v}\right\|_1 + \frac{\beta}{\gamma} \sum_{j=1}^{2} \|v_j\|_{TV} \, dt.$$

These subproblems are linear and convex.

[Burger, Dirks, Frerking, Hauptmann, Helin & S, submitted]

We simulate a “pinball phantom”

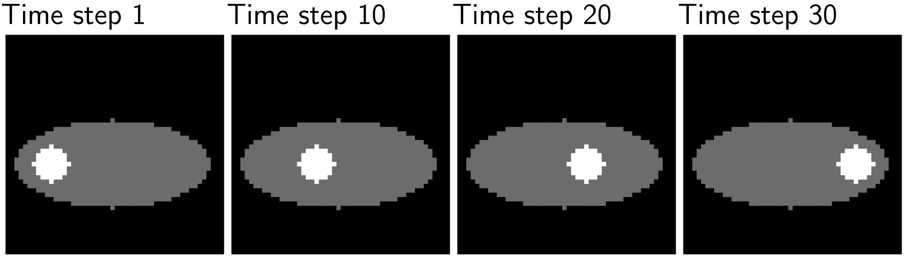

[Burger, Dirks, Frerking, Hauptmann, Helin & S, submitted]

Reconstructions with L^1 data fidelity

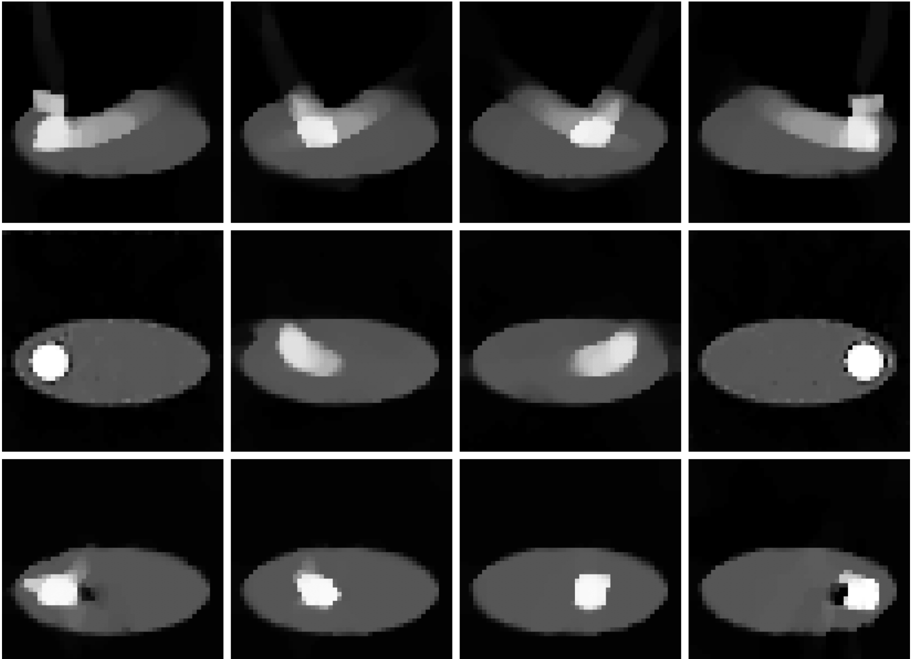

Reconstructions with L^2 data fidelity

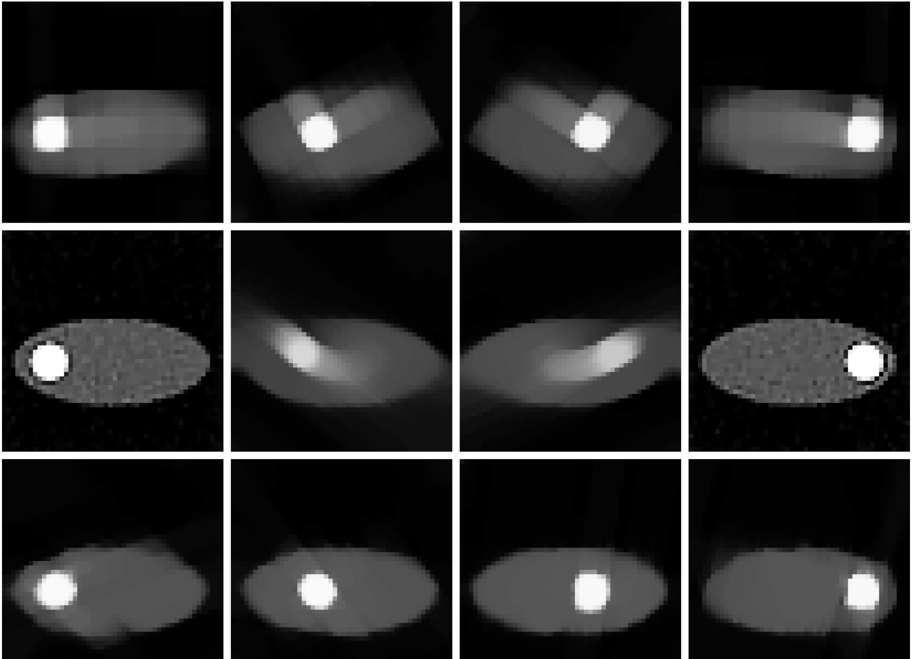

Outline

Total variation regularization: parameter choice
- Background
- Computational examples
- How about theory?

X-ray tomography for moving objects
- Introduction to the problem
- Spacetime level set method
- Shearlet sparsity in spacetime
- Optical flow
- Kalman filter
- Comparison of methods

This part of the talk is a joint work with

Janne Hakkarainen, University of Helsinki, Finland

The principle of Kalman filtering

Consider a pair of time-dependent state x_k and observations y_k:

$$\begin{cases} x_k & = \mathcal{M}_k(x_{k-1}) + \xi_k, \\ y_k & = \mathcal{H}_k(x_k) + \varepsilon_k, \end{cases}$$

where $\mathcal{M}\colon \mathbb{R}^n \to \mathbb{R}^n$ is the dynamical state space model and $\mathcal{H}\colon \mathbb{R}^n \to \mathbb{R}^p$ is the observation operator that maps from the state space to the observation space. The terms ξ_k and ε_k model errors. Probabilistic notation:

$$\begin{cases} x_k & \sim p(x_k | x_{k-1}), \\ y_k & \sim p(y_k | x_k). \end{cases} \tag{1}$$

In filtering, our aim is to find the posterior distribution $p(x_k | y_{1:k})$ of the state, given all the previous and current observations $y_{1:k}$ using Bayesian inference.

Kalman filtering in the Gaussian case

In linear Kalman filtering, the state estimate x_{k-1}^{est} of the previous time-step and its error covariance matrix C_{k-1}^{est} are transported to the next time-step's prior x_k^p using linear model M_k

$$\begin{aligned} x_k^p &= M_k x_{k-1}^{est}, \\ C_k^p &= M_k C_{k-1}^{est} M_k^{\mathcal{T}} + Q_k, \end{aligned}$$

where Q_k is the model error covariance matrix. The innovation (prediction residual) and its error covariance matrix are

$$\begin{aligned} r_k &= y_k - H x_k^p, \\ C_k^r &= H_k C_k^p H_k^{\mathcal{T}} + R_k, \end{aligned}$$

where R_k is the observation error covariance matrix. Update step:

$$\begin{aligned} x_k^{est} &= x_k^p + G_k r_k, \\ C_k^{est} &= (I - G_k H_k) C_k^p, \end{aligned}$$

with Kalman gain matrix $G_k = C_k^p H_k^{\mathcal{T}} (C_k^r)^{-1}$.

Outline

We construct a dynamic "emoji phantom" using small stones and stop-motion animation

Measurement:
Zenith Purisha

We construct a dynamic "emoji phantom" using small stones and stop-motion animation

Measurement:
Zenith Purisha

We construct a dynamic “emoji phantom” using small stones and stop-motion animation

Measurement:
Zenith Purisha

We construct a dynamic "emoji phantom" using small stones and stop-motion animation

Measurement:
Zenith Purisha

We construct a dynamic “emoji phantom” using small stones and stop-motion animation

Measurement:
Zenith Purisha

We construct a dynamic "emoji phantom" using small stones and stop-motion animation

Measurement:
Zenith Purisha

We construct a dynamic "emoji phantom" using small stones and stop-motion animation

Measurement:
Zenith Purisha

We construct a dynamic "emoji phantom" using small stones and stop-motion animation

We construct a dynamic "emoji phantom" using small stones and stop-motion animation

Measurement:
Zenith Purisha

We construct a dynamic “emoji phantom” using small stones and stop-motion animation

Measurement: Zenith Purisha

We construct a dynamic “emoji phantom” using small stones and stop-motion animation

Measurement: Zenith Purisha

We construct a dynamic “emoji phantom” using small stones and stop-motion animation

Measurement:
Zenith Purisha

We construct a dynamic "emoji phantom" using small stones and stop-motion animation

Measurement:
Zenith Purisha

We construct a dynamic "emoji phantom" using small stones and stop-motion animation

Measurement:
Zenith Purisha

We construct a dynamic "emoji phantom" using small stones and stop-motion animation

Measurement:
Zenith Purisha

Demonstration of dynamic tomography methods

https://www.youtube.com/watch?v=JTdVAQTFKxI

Demonstration of the Kalman filter approach

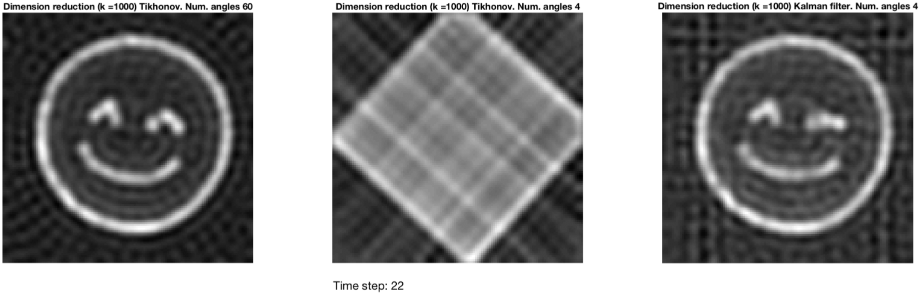

Show Kalman filter emoji movie by Janne Hakkarainen!

Thank you for your attention!